molecules

MDPI

Article

Inhibition of Q235 Carbon Steel by Calcium Lignosulfonate and Sodium Molybdate in Carbonated Concrete Pore Solution

Bing Lin and Yu Zuo *

Beijing Key Laboratory of Electrochemical Process and Technology for Materials, Beijing University of Chemical Technology, Beijing 100029, China; 2015400068@mail.buct.edu.cn

* Correspondence: zuoy@mail.buct.edu.cn; Tel.: +86-010-64423795

Received: 4 January 2019; Accepted: 30 January 2019; Published: 31 January 2019

Abstract: The inhibition effect and mechanism of a compound calcium lignosulfonate (CLS) and sodium molybdate inhibitors for Q235 carbon steel in simulated carbonated concrete pore solution (pH 11.5) with 0.02 mol/L NaCl are studied using electrochemical and surface analysis techniques. The results show that in carbonated simulated concrete pore (SCP) solution CLS and Na_2MoO_4 show a synergistic inhibition effect. The compound inhibitor can be defined as mix-type inhibitor. With 400 ppm CLS plus 600 ppm Na_2MoO_4, the pitting potential moves positively about 200 mV, and the inhibition efficiency reaches 92.67%. After 24 h immersion, the IE% further increases up to 99.2%. The surface analysis results show that Na_2MoO_4 could promote stability of the passive film, and the insoluble molybdenum compounds and $CaO/Ca(OH)_2$, together with adsorbed CLS, deposit on the steel surface, forming a complex film. The compounded film effectively inhibits corrosion of the steel.

Keywords: carbonated concrete environment; carbon steel; calcium lignosulfonate (CLS); sodium molybdate; synergistic effect; corrosion experiments; inhibition

1. Introduction

Reinforced concrete is the most widely used construction material [1–3], while corrosion of reinforcing steel is the main reason leading to the premature deterioration of reinforced concretes [4,5]. Corrosion of reinforcing steel is related to the carbonation of concrete [2,3,6] and the presence of chloride ions [7,8]. The carbonation of concrete is the result of CO_2 diffusion and reaction with the hydrated product ($Ca(OH)_2$), which leads to the composition change of the concrete pore solution and the decrease of pH value. Several techniques have been employed to reduce corrosion of reinforcing steel, among which corrosion inhibitor is the most practical method owing to its advantages of low cost, high efficiency, and wide applicability [1–3,9–11]. For example, $Ca(NO_2)_2$ is an inorganic corrosion inhibitor commonly used in reinforced concrete construction [12–14]. NO_2^- could help to form a uniform passive film on a steel surface [13,14] and prevent the steel from corroding. However, most of the commercial inhibitors remain unfriendly to the environment. In recent years, researchers have paid considerable attention towards the development of various more effective and greener inhibitors to prevent the corrosion of rebars [15,16].

Lignosulfonates (LS) are the by-products of the pulping waste liquor in acid sulfite pulp mills [17]. One of the most common applications of lignosulfonates is as dispersing agents and set-retarding agents in concretes [18]. As corrosion inhibitors, lignin-based compounds contain plenty of hydroxyl, carboxyl, or methoxyl groups, which can be adsorbed onto a metal surface by sharing their lone pair electron or π-electron with the free d-orbital of metal. In acidic solution, the inhibition efficiency of lignin and its modifications for steel depend on the number of carboxy groups in the

macromolecule [19], the inhibitor concentration, and the environmental factors [20]. In neutral aqueous solutions with Cl^-, lignin monomers acted as mixed type inhibitors on steel corrosion [21] and the inhibitive performance of lignin derivatives depended on their functional groups [22]. Bishop et al. [23] have confirmed that the $–SO_3$ and –OH groups present in LS can be adsorbed on a steel surface and generate an impermeable structure. Li et al. [24] revealed that LS adsorbed in the form of aggregates and the adsorption isotherm follows the Freundlich model at low pH values. In neutral solutions, LS increasingly adsorbed on steel in the form of well separated single molecules, which can be well fitted using the Langmuir equation. However, there is little research involving calcium lignosulfonate (CLS) as a corrosion inhibitor in alkaline solution. Our work [25] showed that CLS is a good corrosion inhibitor in saturated $Ca(OH)_2$ solutions with Cl^- for carbon steel. The adsorption film on a steel surface is formed by both physisorption and chemisorption. Particularly, CLS could be preferentially adsorbed on the active sites on a steel surface using the sinapyl alcohol group, which is beneficial to the inhibition of pitting corrosion.

Molybdate is an environment-friendly anodic passivation inhibitor [26,27]. The inhibition mechanism of molybdates has been studied by many scholars, and competitive adsorption [28], adsorption film [27,29], and oxidation [30] are the dominant views. In order to enhance the inhibition effective of molybdates, some authors [31–33] tried to associate Na_2MoO_4 with organic inhibitors. It was reported [33] that the synergistic effect is present between molybdate and benzotriazole (BTA). The compounded inhibitor could promote the transformation of FeOOH and Fe_2O_3 in the passive film, and both passivation and pitting corrosion resistance were promoted.

On the other hand, most studies focusing on inhibitors for reinforcing steel were performed with high pH concrete pore solutions. The carbonation of concretes would directly affect the passivation film on reinforcing steel surfaces, but few studies were carried out in carbonated concrete environments. In the present work, the combined inhibition effect of CLS and molybdate on Q235 carbon steel in simulated carbonated concrete pore solution is studied with electrochemical measurements and surface analysis methods. Particularly, the synergistic effect between Na_2MoO_4 and CLS is paid attention to.

2. Results and Discussion

2.1. Inhibition Evaluation

2.1.1. Potentiodynamic Polarization Measurement

Figure 1a shows the polarization curves of Q235 carbon steel after immersion in test solutions without and with various concentrations of CLS. The polarization curves show typical passivation-pitting corrosion behavior. Figure 1b shows the electrochemical parameters obtained from the polarization curves.

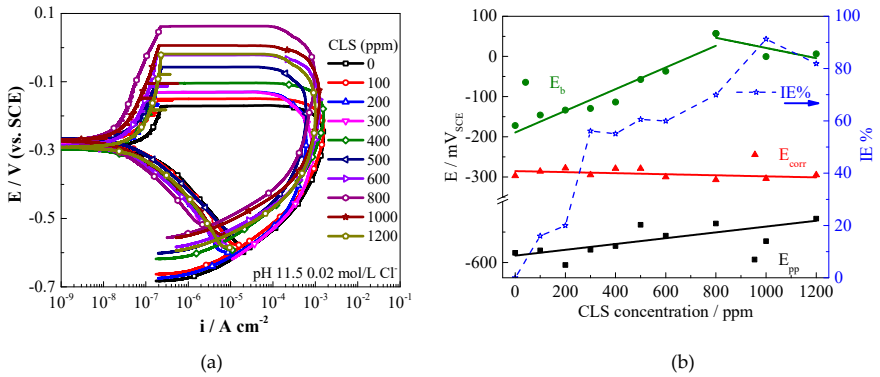

(a) (b)

Figure 1. (**a**) Polarization curves of Q235 carbon steel in simulated concrete pore (SCP) solution with various concentration of calcium lignosulfonate (CLS); (**b**) Electrochemical parameters based on the polarization curves.

The corrosion potential (E_{corr}) of carbon steel in the test solution is about −290 mV_{SCE}, and almost has almost no change as CLS concentration increases, indicating CLS acts as a mixed-type inhibitor [34,35]. The inhibition efficiency (IE%) increases as the CLS concentration increases, which is consistent with the results of other authors [17,25]. As an organic inhibitor, CLS could form an adsorption film on a steel surface [25], which has a barrier effect to prevent general corrosion. The pitting potential (E_b) is the potential at which the anodic current increases rapidly [36], and the localized corrosion starts above this potential. As the CLS concentration increases from 100 to 800 ppm, the E_b value increases from -146 mV_{SCE} to 57 mV_{SCE}, and then slightly decreases. This result indicates that the pitting corrosion susceptibility of carbon steel decreases as the inhibitor concentration increases. The max current density (i_{peak}), which is related to the growth rate of the corroded pits [37], remains almost unchanged as the CLS concentration increases. The repassivation potential (E_{pp}) is the intersection potential of the forward and reverse scans, and the steel potential must be above E_{pp} for existing areas of localized corrosion to propagate [38]. As the CLS concentration increases the E_{pp} shows relatively smaller shifts to positive, compared with the obvious shifts of the E_b values. The results of i_{max} and E_{pp} reveal that, as a corrosion inhibitor, CLS has little effect on the repassivation process of carbon steel. Compared with the inhibition effect of CLS in pH 12.5 concrete pore solution [25], the inhibition ability of CLS in carbonated SCP solution decreases for both general corrosion and localized corrosion. Therefore, the combination of CLS with other inhibitors to improve the inhibition effect is necessary.

Figure 2 shows the polarization curves and the electrochemical parameters of Q235 steel in test solution with various concentrations of Na_2MoO_4. The E_{corr} slightly increases with the increase of MoO_4^{2-} concentration, indicating that Na_2MoO_4 acts as a mixed-type inhibitor [34,35] predominantly with anodic effectiveness [39]. Na_2MoO_4 is a moderate inhibitor for general corrosion, and the IE% increases as the Na_2MoO_4 concentration increases. The passive current density decreases obviously with the increase of the inhibitor concentration, indicating Na_2MoO_4 promoted passivation of the steel. $Fe_2(MoO_4)_3$ complex is insoluble and protective in neutral and alkaline media [29], which could enhance the protection film formed on steel surfaces [39]. Refaey et al. [40] reported that the formation of a protective film played a critical role on the inhibition effect of molybdate. The increased E_b and passivation region (E_b-E_{corr}) due to the increase of MoO_4^{2-} concentration might be associated with the effect of molybdate reducing the number and magnitude of metastable pitting transients [39,41]. In other words, molybdate ions could block the active sites on the surface [42] and affect the nucleation of pits by deactivating or reducing the number of sites, leading to decreased pitting corrosion susceptibility [43]. As shown in Figure 3, on the reverse scan, a potential step, the pit transition potential (E_{ptp}) [39,44,45], is detected for steel in the test solution with molybdate. The E_{ptp} is a characteristic potential that is correlated with repassivation at the pit bottom [44,45], which might lead to the concentration gradients for mass transport and promote further pit nucleation. In the pit environment, a series of chemical reactions involving hydrolysis and polymerization of molybdates may occur as the pH value decreases [29,46]:

$$7MoO_4^{2-} + 8H^+ \rightarrow Mo_7O_{24}^{6-} + 4H_2O \quad (1)$$

$Mo_7O_{24}^{-}$ has a chelate effect with iron(III) to form complexes, which could help repassivation of the pit. In Figure 2b, the E_{ptp} potential increases as the molybdate concentration increases, which means that molybdate with relatively higher concentration could help to form a repassivation film at the pit bottom.

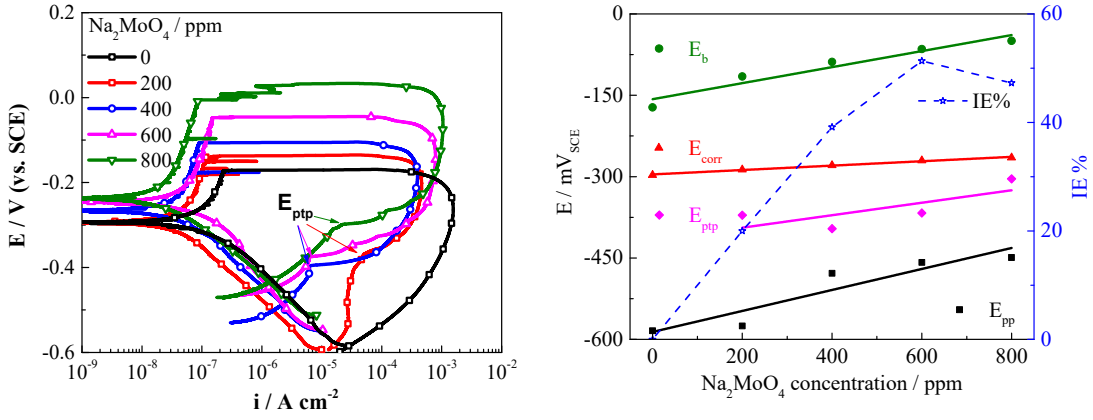

Figure 2. (**a**) Polarization curves of Q235 carbon steel in SCP solutions with various concentrations of Na_2MoO_4; (**b**) The electrochemical parameters based on the polarization curves.

The mechanism of molybdate inhibition in carbonation SCP solution could be inferred. In the first step, the MoO_4^{2-} ions competitively adsorb on the steel surface with Cl^- ions [47,48]. Then the passivation film could be enhanced by the adsorbed molybdate ions [49] and a precipitation film composed of oxidized molybdenum forms on the steel surface. The composite film could increase both the general corrosion and pitting corrosion resistances. However, once the pits occur, MoO_4^{2-} cannot stop the pit growth and self-catalyzed corrosion occurs inside the pits which accelerates the growth of pits.

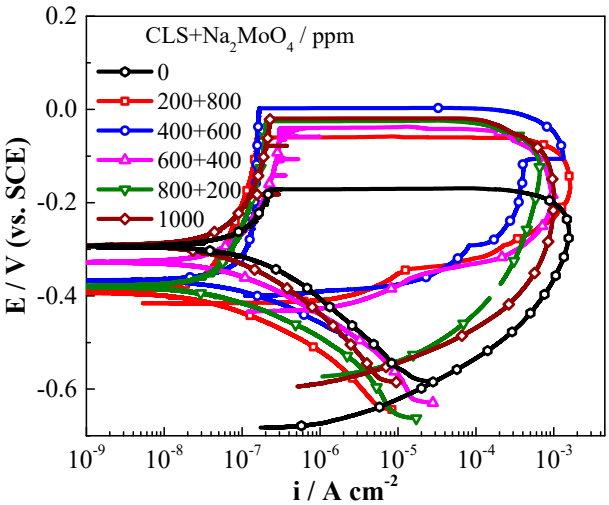

Figure 3. Polarization curves in solutions with different ratios of CLS and Na_2MoO_4.

Figure 3 shows the cyclic potentiodynamic polarization (CPP) curves of Q235 carbon steel in carbonated SCP solution with different ratios of CLS and Na_2MoO_4 (total 1000 ppm), and the electrochemical parameters are shown in Table 1. The E_{corr} slightly increases as the CLS ratio increases, which is the same as the result of molybdate compound with glycol [47]. The compound inhibitor acts as a mix-type inhibitor with predominantly anodic effectiveness [47]. The IE% slightly decreases as the CLS ratio increases. The synergistic parameter (S), which reveals the interaction relationship between CLS and Na_2MoO_4, is calculated using the following equation [50,51]:

$$S = \frac{1 - IE\%_{(1+2)}}{1 - IE\%_c} \quad (2)$$

where $IE\%_{(1+2)} = (IE\%_1 + IE\%_2) - (IE\%_1 \times IE\%_2)$, and $IE\%_1$, $IE\%_2$, and $IE\%_c$ are the inhibition efficiencies for CLS, Na_2MoO_4, and CLS/Na_2MoO_4 compound, respectively. The calculated S values are all above 1, indicating the synergistic behavior of the selected inhibitor combination [50], and the S value increases as the CLS concentration decreases, which means the synergistic effect between the two inhibitors decreases. The obtained E_b potentials for each compound inhibitor ratios are relatively close and obviously higher than the value without inhibitor. The compound with 400 ppm CLS and 600 ppm Na_2MoO_4 shows the highest E_b. The E_{pp} significantly increases as the CLS ratio decreases, which means that a decrease of the CLS ratio in the compound inhibitor could promote the repassivation of carbon steel, while adding CLS or molybdate alone does not show this promoting effect. The difference between E_b and E_{pp} represents the repassivation tendency of pits on steel surface, which decrease as the molybdate concentration increases. This result suggests that the high ratio of molybdate in the compound inhibitor would be beneficial to inhibit localized corrosion. It has been reported that pitting corrosion could not be inhibited and might even be promoted if the molybdate concentration is too low [52,53]. This might be attributed to the pH changes in the pit environment in which the pH cannot be raised enough to passivate the pit [27,52]. The above results show that the compound inhibitor effectively increases both the general corrosion resistance and the pitting corrosion resistance, and the optimum ratio is 400 ppm CLS compound with 600 ppm Na_2MoO_4.

Table 1. Electrochemical parameters of Q235 steel in carbonated SCP solution with different ratios of CLS and Na_2MoO_4 using cyclic potentiodynamic polarization (CPP) measurements.

Inhibitor		E_{corr}	E_b	E_{pp}	**IE%**	**S**
CLS	Na_2MoO_4	mV_{SCE}	mV_{SCE}	mV_{SCE}		
0	0	−298	−171.2	−584	–	–
200	800	−375	−73.2	−407	93.88	6.89
400	600	−338	3.9	−399	92.67	2.98
600	400	−310	−43.8	−429	81.73	1.34
800	200	−364	−15.3	−577	78.33	1.11
1000	0	−304	−0.3	−565	91.27	–

The pre-filming time has an important role in the inhibition processes [54,55]. CLS could form an adsorption film on a steel surface after 10 h pre-filming in concrete pore solution, which could reduce the content of Cl^- adsorbed on the steel surface and prevent the local enrichment of Cl^- [25]. As shown in Figure 4a, for the samples immersed in solution without inhibitor, with extended immersion time, E_{corr} decreased and i_{corr} increased obviously, and the passivation behavior disappeared. While for the samples with compound inhibitor, shown in Figure 4b, the polarization curves show typical passivation-pitting behavior. As the pre-filming time increases the E_{corr} increases, the i_{corr} decreases, and the IE% (calculated by i_{corr}) increases from 92% to 99%. This result reveals that the compound inhibitor could enhance the general corrosion resistance after pre-filming time. E_b for the inhibited steels obviously increases as the immersion time increases, while the E_{pp} shows almost no shift, which suggests that in the carbonated solution the inhibitor could help Q235 steel maintain and improve the passivation state as the pre-filming time increases, especially for the first 16 h. The results confirm the good inhibition effect of the compound inhibitor after pre-filming time on both general corrosion and localized corrosion.

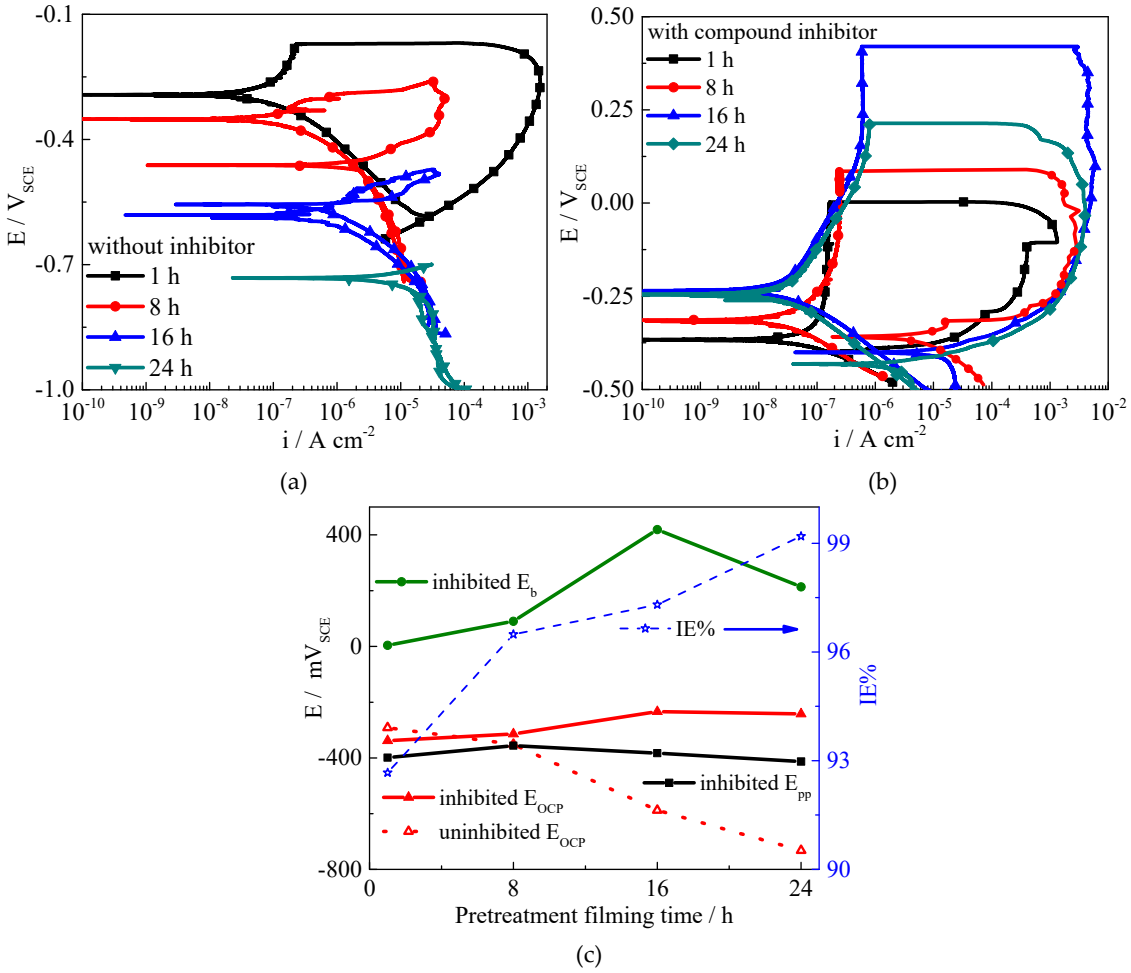

Figure 4. Polarization curves and parameters of Q235 steel immersed in carbonated SCP solution for various times, (**a**) without inhibitor, (**b**) with compound inhibitor, (**c**) electrochemical parameters obtained based on polarization curves.

2.1.2. Electrochemical Impedance Spectroscopy Measurements

To investigate the inhibitive behavior of CLS, Na_2MoO_4, and the compound inhibitor, a series of EIS tests were performed in carbonated SCP solution with various concentrations of different inhibitors. As shown in Figure 5, a single depressed capacitive semicircle is presented in all the Nyquist plots, and the capacitive semicircle radius increases as the inhibitor concentration increases. This result reveals that the addition of inhibitor did not change the mechanism of the corrosion process but inhibited corrosion by forming protective film on the steel surface [56]. The inhibitive system could be described using the model of the solution/steel interface, as shown in Figure 5d. In the equivalent circuit, R_s is the solution resistance and R_{ct} represents the charge-transfer resistance corresponding to the corrosion reaction at the metal substrate/solution interface. R_{film} and C_{film} represent the resistance and the capacitance of the protection film, respectively. The constant phase angle elements (CPE) is used in the model to compensate for the non-homogeneous electrode surface. The fitted parameters are shown in Figure 6.

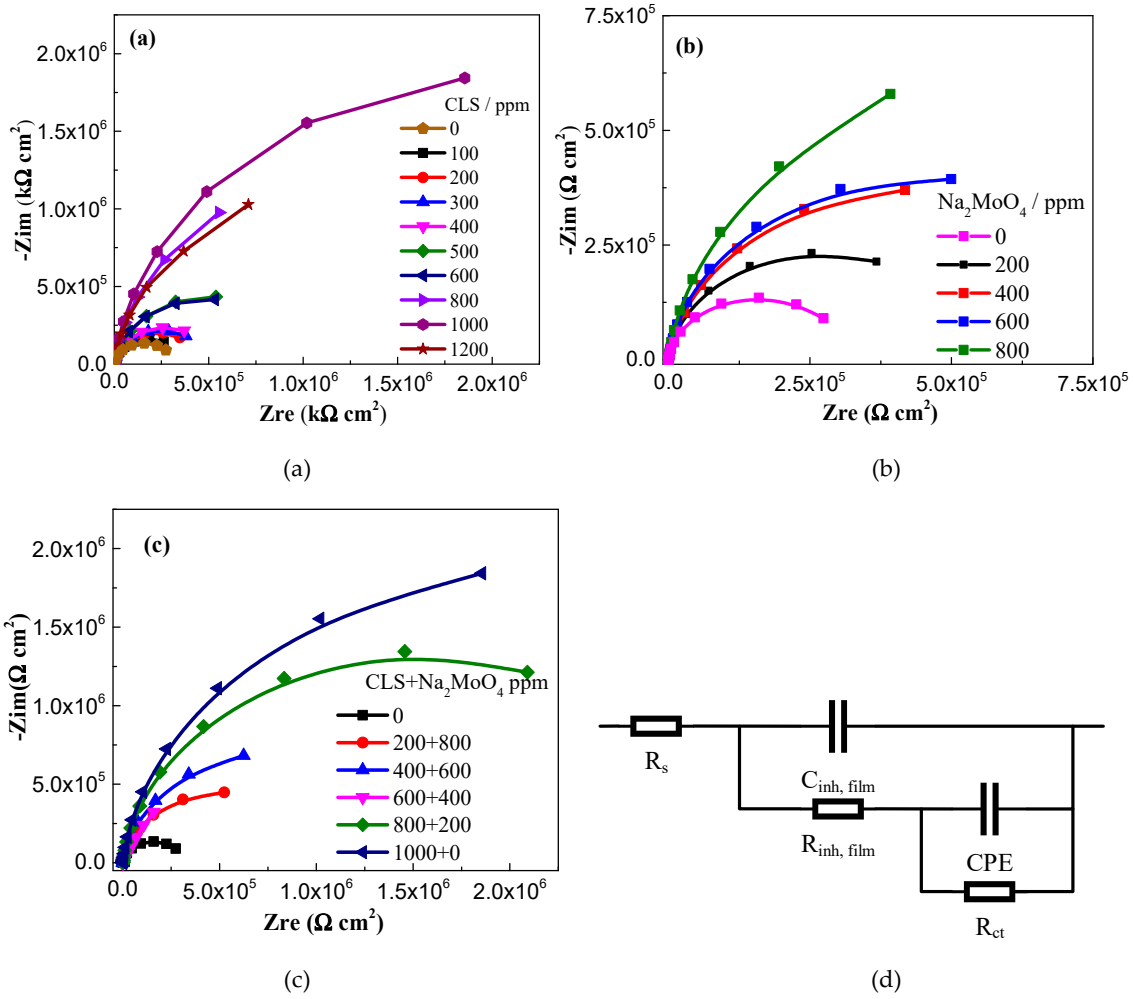

Figure 5. Nyquist plots of Q235 carbon steel in test solutions, (**a**) with CLS; (**b**) with Na_2MoO_4; (**c**) with optimal ratio of CLS and Na_2MoO_4; (**d**) the equivalent circuit.

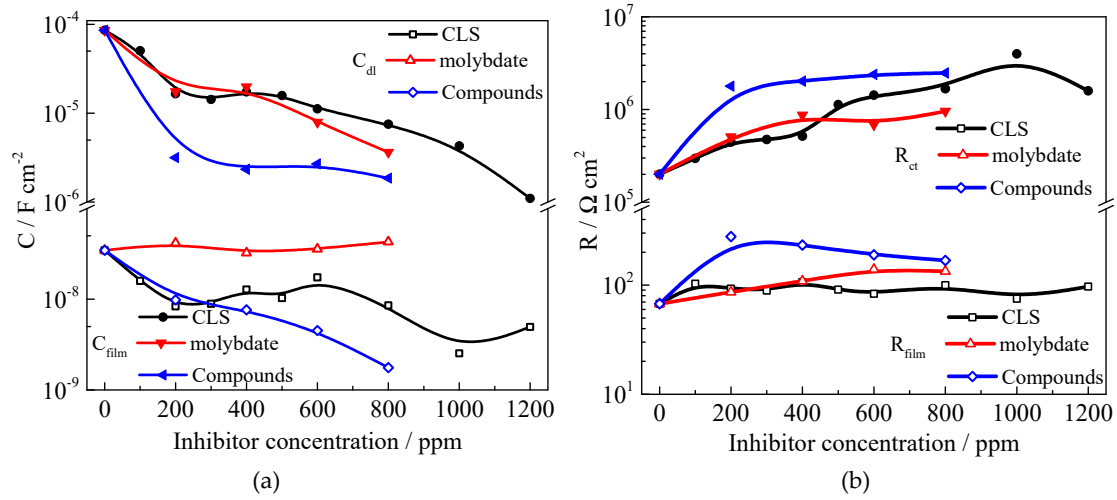

Figure 6. Electrochemical parameters of Q235 steel in carbonated SCP solution with different concentrations of inhibitor using electrochemical impedance spectroscopy (EIS) measurements, (**a**) C_{dl} and C_{film}; (**b**) R_{ct} and R_{film}.

Figure 5a shows the Nyquist plots of samples immersed in test solution with various concentrations of CLS. As the CLS concentration increases the diameter of the capacitive loop increases

obviously. This phenomenon might be due to the increase of surface coverage by the adsorbed inhibitor film [56]. From the parameters in Figure 6, the R_{ct} increases and the R_{film} shows almost no shift as the CLS concentration increases, which suggests that the corrosion reaction was inhibited by the adsorption CLS film on the steel surface. The C_{dl} decreases as the CLS concentration increases, indicating that the status of the steel/solution interface has been changed by the adsorption of CLS. Furthermore, the C_{film} decreases with increased CLS ratio in the compound inhibitor. According to the Helmholtz model, the capacitance is inversely proportional to the surface changes [50,56]:

$$C = \varepsilon_0 \varepsilon S/d \quad (3)$$

where d is the film thickness, S is the surface area of working electrode, ε_0 is the permittivity of air and ε the local dielectric constant [56–58]. The decrease of C_{dl} and C_{film} might be attributed to the replacement of the adsorbed water molecules at the metal surface by CLS molecules, which have a lower dielectric constant. The adsorbed CSL film and the passive film could form a double-layer barrier on the steel surface [25]. As the CLS concentration increased the adsorbed CLS molecules increased, resulting in a dense and homogeneous inhibition film on the steel surface.

From Figures 5b and 6, it can be seen that the C_{dl} decreases and the R_{ct} increases as the Na_2MoO_4 concentration increases, which means molybdate could increase the corrosion resistance to decrease the corrosion rate. As the molybdate concentration increases, the C_{film} value has almost no shift, and the R_{film} increases significantly. The EIS results confirm that a barrier layer, depending on the concentration of molybdate, blocked the adsorption of Cl^- [29]. In addition, molybdate could enhance the passivation film to protect the steel. Gong et al. [59] reported that molybdate enhances the self-healing ability of passive films, thereby leading to improvement of corrosion resistance.

After adding compound inhibitor, the Nyquist plots are shown in Figure 5c and the parameters are displayed in Figure 6. As the CLS ratio increases, the C_{dl} decreases slightly and the R_{ct} almost has no change, again indicating that the compound inhibitor could increase the corrosion resistance. The C_{film} value significantly decreases and the R_{film} value decreases slightly. In the compound inhibitor, the barrier effect of the protective film increases as the CLS ratio increases, and the passive film is enhanced to prevent corrosion as the molybdate ratio increases. The results revealed the compound inhibitor has a better inhibition effect for carbon steel in test solution.

In order to confirm the effect of pre-filming time on inhibition of the compound inhibitor, EIS measurements for Q235 carbon steel in the test solution with compound inhibitor for various immersion times were carried out and the results are shown in Figure 7. As the immersion time increases the diameter of the capacitive loop increases, which means as the pre-filming time increases the inhibition effect increases, which might be due to the increase in the surface coverage [56] or in the thickness of the protection film. From the EIS parameters shown in Figure 7b, the C_{film} decreases obviously and the R_{film} slightly increases as the immersion time increases, which also suggests the formation of adsorption film on the steel surface. In addition, the decreased C_{dl} and increased R_{ct} indicate that the corrosion reactions have been suppressed by the inhibitor. The above results confirm the results of the polarization measurements and suggest that after 16 h to 24 h pre-filming the compound inhibitor would show better inhibition effect.

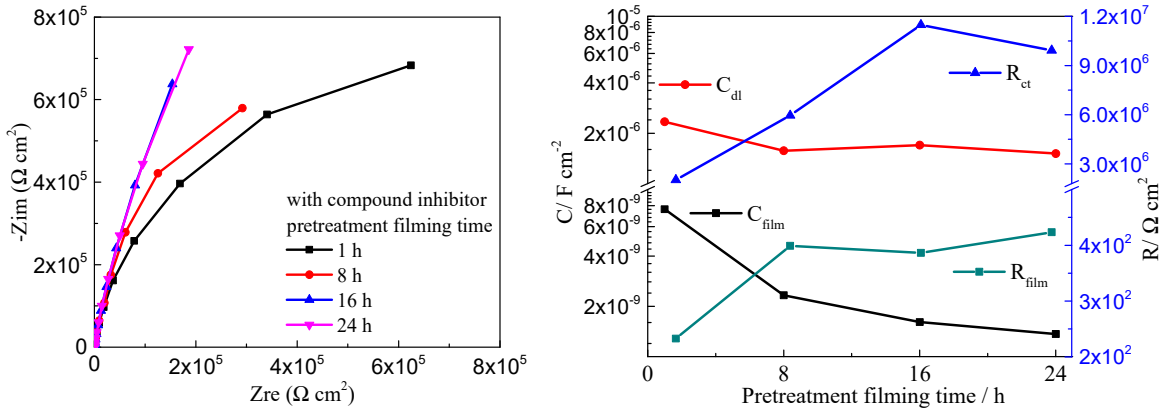

Figure 7. Nyquist polts (**a**) and EIS parameters (**b**) of Q235 steel in test solution with different pretreatment filming time.

2.2. Surface and Isotherm Adsorption Studies

2.2.1. X-ray Photoelectron Spectroscopy Measurement and Contact Angle

In order to determine the chemical composition of the inhibited surface, XPS analyses were used to characterize the Q235 carbon steel after 1 h immersion in carbonated SCP solutions with 800 ppm CLS, 800 ppm Na_2MoO_4, and 400 ppm CLS, plus 600 ppm Na_2MoO_4, respectively. The obtained high-resolution peaks for Ca 2p, C 1s, O 1s, S 1s, Fe 2p, and Mo 3d core levels are fitted and shown in Figures 8–10.

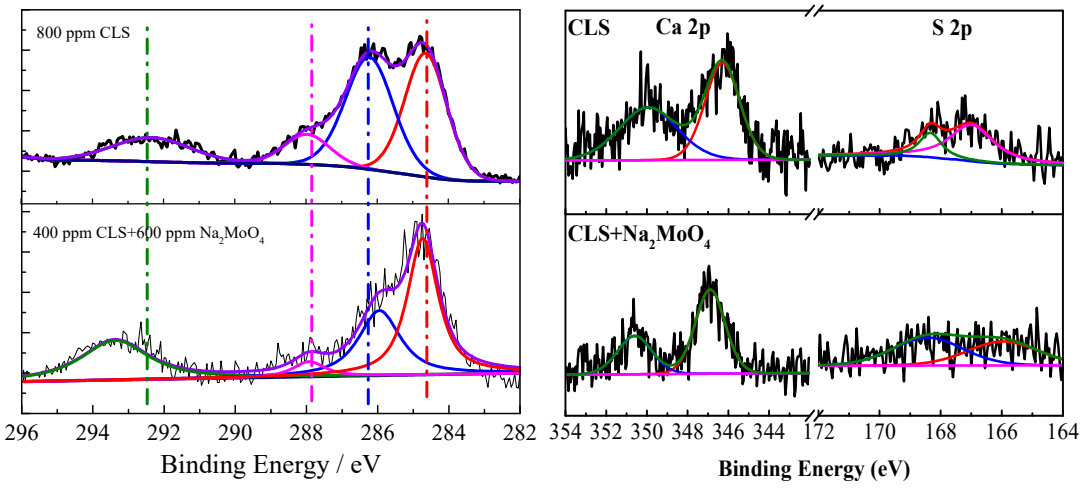

Figure 8. High-resolution XPS spectrum of Q235 steel immersed in test solution with CLS and CLS+Na_2MoO_4: (**a**) C 1s; (**b**) Ca 2p and S 2p.

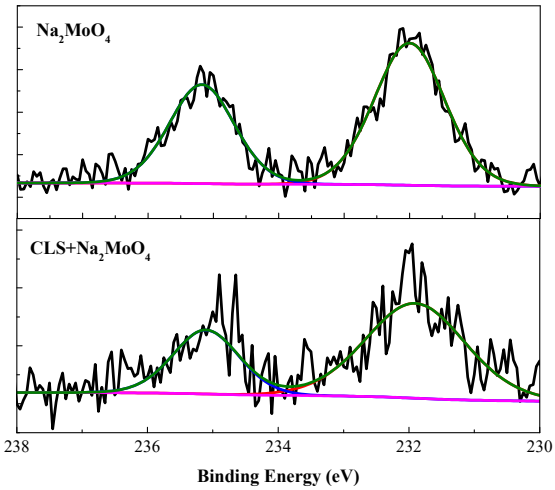

Figure 9. High-resolution XPS spectrum of Mo 3d for Q235 carbon steel immersed in carbonation SCP solution with Na_2MoO_4 and CLS+Na_2MoO_4.

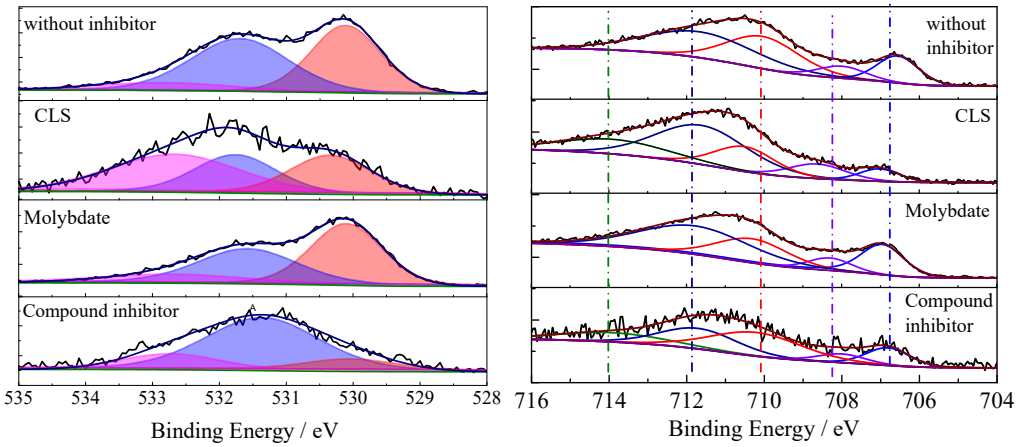

Figure 10. High-resolution XPS spectrum of Q235 carbon steel immersed in carbonation SCP solution with different inhibitors: (**a**) O 1s; (**b**) Fe 2p.

In Figure 8a, the C 1s spectra for CLS and compound inhibitor treated steel surface shows four peaks. The peak at 284.8 eV and 287.9 eV can be attributed to the C-C/C-H bonds [35,44,60] and the C-O bonds [50,61] in CLS molecules, respectively. The peak at 286.4 eV may be assigned to the carbon atom bonded to S in C-S bonds [60]. This peak on the compound inhibitor treated surface shifts negatively to 286 eV, suggesting that the adsorbed CLS may accept the feedback electrons from Fe atoms on the surface. The last peak at 292.2 eV can be attributed to the benzene ring in the organic inhibitor [60,61]. This peak shifts positively to 293.4 eV on the compound inhibitor treated surface, indicating the aromatic ring of the CLS supplied electrons to Fe atoms [62]. Figure 9 presents the Ca 2p and S 2p spectra for the CLS and compound inhibitor treated sample. Ca and S are the characteristic elements in CLS, which could confirm the adsorption of CLS. The Ca2p spectrum is decomposed into two peaks at 351 eV and 347.4 eV, which are attributed to $CaO/Ca(OH)_2$ [25,63] and Ca-O-S bonds [25] on the steel surface, respectively. This result suggests the $CaO/Ca(OH)_2$ has been precipitated on the steel surface and could enhance the adsorption of CLS by forming Ca-O-S bonds [25] to form a more complete film on the surface. For S 2p, there are two peaks. The first one is the peak at 168.4 eV [25,50] attributed to Ca-O-S, and the co-adsorption of CLS and Ca could protect the surface from corrosion [25,60,64]. On the compound inhibitor treated surface, this peak is widened, which

might be due to the M-S-O bonds, where M could be Ca^{2+}, Fe^{2+}, or Fe^{3+}. The area ratio of M-O-S on the compound inhibitor treated sample is much larger than that on the CLS treated sample, which means molybdate could enhance the adsorption of LS^{2-}. The other peak at 167 eV [25,50] can be attributed to S in the organic inhibitor. The above XPS results confirm the adsorption of CLS and reveal the precipitation of oxides or hydroxides of Ca and Mo, which could help to enhance the adsorption of the organic inhibitor.

As shown in Figure 9, the high-resolution Mo 3d spectra are detected on both the surface treated using Na_2MoO_4 and the compound inhibitor. The two peaks at 231.9 eV is attributed to Mo^{4+}, such as MoO_2 [62], and the peak at 235.1 eV is the peak of Mo^{6+} [33], which could confirm the precipitation of MoO_x and adsorption of molybdate on the surface. The passive film formed by the reduction of molybdate mainly consists of iron oxide and molybdenum oxide. The reduction of Mo^{6+} could help to form a more stable film [47,65].

The O1s peaks for Q235 carbon steel immersed in test solutions with different inhibitors are shown in Figure 10a. The first peak at 530.1 eV corresponds to O^{2-}, which could be attributed to the bond with Fe^{3+} in Fe_2O_3, Fe_3O_4, or MoO_4^{2-} [33,35]. The second peak at 531.6 eV can be attributed to the metal oxides and hydroxides or H_2O species on the steel surface [35,66]. The third peak may be assigned to the oxygen atoms of the O-C bond in the organic compounds from surface contamination and from the adsorbed water at 532.7 eV [60,62]. The deconvolution of the high-resolution Fe 2p3/2 spectra of the steel surface treated using different inhibitors show several peaks, which are shown in Figure 10b. The first component at 706.8 eV is attributed to metallic iron (Fe^0) [35]. The peaks at 708.3 eV and 710.4 eV can be attributed to the Fe^{2+} present in FeO [35,39] and Fe_3O_4 [60], respectively. The peak at 711.5 eV is assigned to Fe^{3+}, which can be associated to the ferric oxide/hydroxide species such as Fe_2O_3, Fe_3O_4, and FeOOH [50,60]. The peak at 714.2 eV is also assigned to Fe^{3+}, which might be related to adsorption of the organic inhibitor [35,67]. In order to understand the effect of immersion time on the composition of passive film, XPS spectra of the samples immersed in the carbonated SCP solution with different inhibitors for different times were measured. The Fe^{3+}/Fe^{2+} ratio could be used to evaluate the stability of the passive film on steel [29], as shown in Figure 11. As the immersion time increases, the Fe^{3+}/Fe^{2+} ratio in the film obtained in solution without inhibitor decreases, indicating that the stability of the passive film decreases with time. For the steel treated using the CLS, the Fe^{3+}/Fe^{2+} ratio slightly decreased in 30 h and then increased, which might be due to the adsorption of CLS replacing water molecules on the steel surface and reducing the passivation tendency. For the molybdate treated sample, the Fe^{3+}/Fe^{2+} ratio increases as the immersion time increases, which confirms the previous result that molybdate could promote passivation of the surface. For the film formed in solution with the compound inhibitor, the Fe^{3+}/Fe^{2+} ratio is the highest for different immersion times. This result also reveals that the combination of CLS and molybdate would further enhance the stability of the passive film.

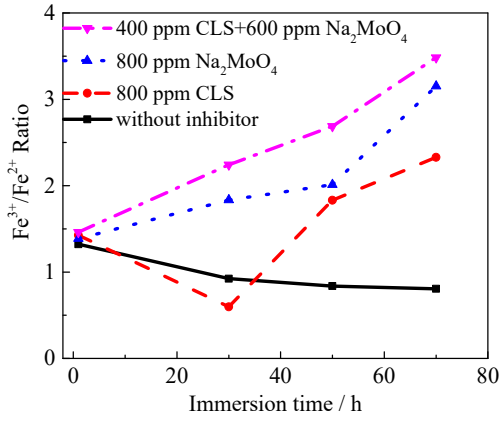

Figure 11. The Fe^{3+}/Fe^{2+} ratio for Q235 steel immersed in test solution with different inhibitors.

The contact angle is an important parameter reflecting the wettability of materials [68,69]. The contact angles of Q235 steel surface treated using different inhibitors for 24 h are shown in Figure 12 and Table 2. The average contact angle for steel immersed in solution without inhibitor is 68.76°, which is consistent with references [68]. The inhibitor pretreatment induced significant changes in the contact angle. CLS causes the contact angle decrease obviously, which might be due to the fact that CLS is a surfactant and the adsorption film formed using CLS contains lots of methoxy, hydroxy, and other hydrophilic groups. The hydrophilic adsorption film could prevent the adsorption of aggressive anions and protect the steel surface [25]. Na_2MoO_4 could slightly increase the contact angle of the steel surface, which might be due to the Mo oxide precipitations decreasing the surface roughness [70]. The contact angle of the compound inhibitor treated steel is about 33.5°, which is between the values of the surface using single inhibitor treatment. The contact angle test results are consistent with the corrosion rate results and reveal the formation of the inhibition film on the steel surface.

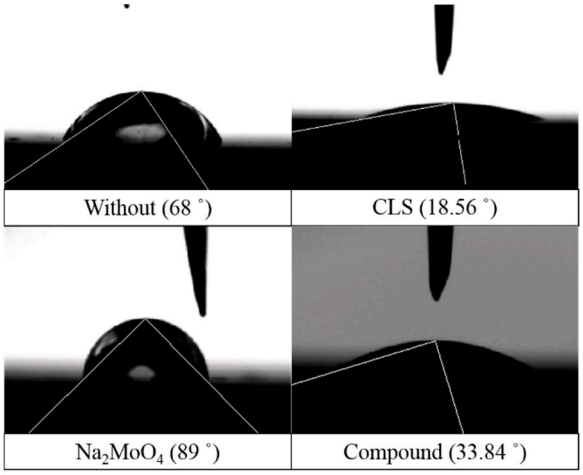

Figure 12. Typical images of water droplets on different inhibitor treated Q235 steel surfaces.

Table 2. Electrochemical parameters of Q235 steel in carbonated SCP solution with different ratios of CLS and Na_2MoO_4 using CPP measurements.

Inhibitor	Contact Angle (Degrees)			Average Contact Angle (Degrees)
	Location 1	Location 2	Location 3	
Without	68.00	66.75	71.54	68.76
CLS	18.32	18.56	16.37	17.75
Na_2MoO_4	85.84	89.00	79.04	84.63
Compound	30.12	33.84	36.42	33.46

2.2.2. Inhibition Mechanism of CLS and Na_2MoO_4 Compound Inhibitor

The inhibition mechanism for the compounded inhibitor could be inferred using the above results, as shown in Figure 13. CLS molecules dissociate instantly to lignosulfonate (LS^{2-}) ions and calcium ions (Ca^{2+}). The steel surface immersed in the SCP solution has extra positive charges, providing a certain driving force for the adsorption of negative (LS^{2-}, MoO_4^{2-}, Cl^-) ions [25,71]. The inhibitor ions (MoO_4^{2-} and LS^{2-}) would adsorb on the steel surface competitively against Cl^- to protect the passive film. The adsorbed molybdate may react with the iron matrix to form Fe^{2+} and MoO_2, and the Fe^{2+} would be further oxidized to form Fe^{3+}. Fe^{3+} could help to form more stable passivation film [29,39] or react with molybdate to form insoluble $Fe_2(MoO_4)_3$. The deposited MoO_2 on steel surface would block the adsorption of Cl^- and prevent the steel from corrosion. Ca^{2+} in alkaline solution can form $Ca(OH)_2$ or CaO, which could precipitate on steel surfaces. Furthermore, the insoluble molybdenum compounds, together with $CaO/Ca(OH)_2$, could precipitate on the passive film to form a complex film,

further enhancing the protection of the film. The precipitated Ca or Mo compounds could also enhance the adsorption of CLS molecules by forming Metal-O-S bonds [25]. Finally, LS^{2-} would adsorb on the outside film, forming a hydrophobic layer to protect the steel.

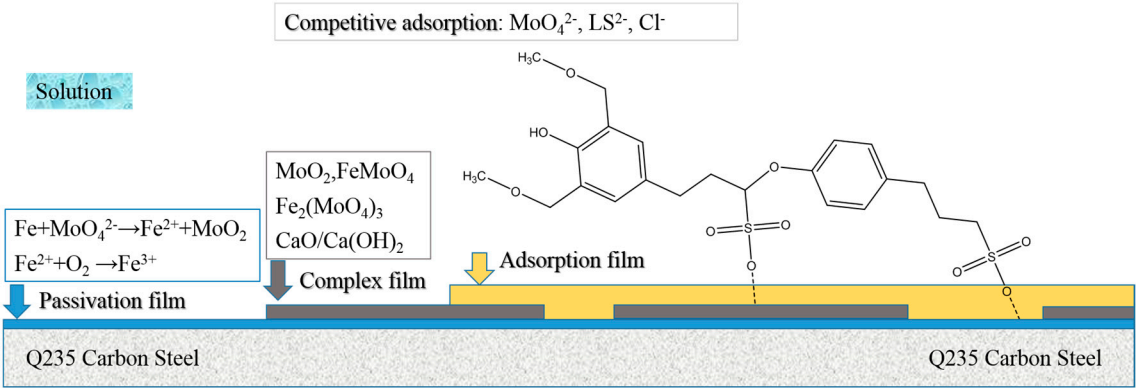

Figure 13. Illustration of the passivation-adsorption structure.

3. Materials and Methods

3.1. Materials and Test Solutions

The studied material was Q235 carbon steel with the following chemical composition (wt%): C 0.13, Si 0.29, Mn 0.76, S 0.11, Cu 0.08, and Fe balance. The sample size was 8 mm × 8 mm × 10 mm. The sample electrode was covered with epoxy resin, leaving a 0.4 cm^2 area exposed to the test solution. The working surface for all samples was abraded with abrasive papers from 240# to 1000#, and cleaned with de-ionized water and ethanol.

The testing solution was composed of 0.0021 mol/L NaOH, 0.0042 mol/L KOH, and 0.02 mol/L NaCl, which was used to simulate the pore solution for a carbonated concrete environment [72]. The calcium lignosulfonate (CLS) and Na_2MoO_4 were analytical grade chemicals. The chemical structure of CLS is shown in Figure 14. The pH value of testing solutions was adjusted to 11.5, and all tests were carried out at room temperature (25 °C).

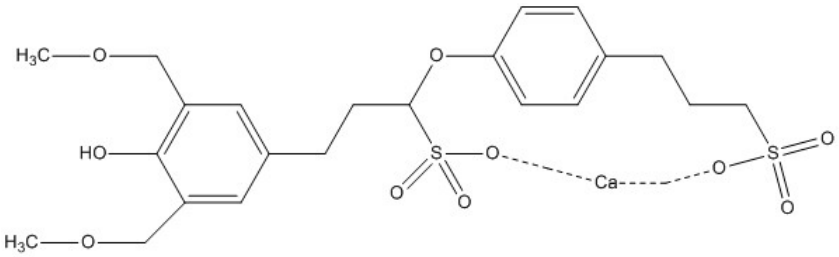

Figure 14. Chemical structure of calcium lignosulfonate (CLS).

3.2. Electrochemical Measurements

Cyclic potentiodynamic polarization (CPP) curves and electrochemical impedance spectroscopy (EIS) were measured using CS350 electrochemical workstation (Corrtest Company, Wuhan, China). The polarization tests were started at a potential 300 mV below the open circuit potential (OCP) at a potential scanning rate of 0.1 mV/s in the anodic direction until the current density increased up to 0.02 mA/cm^2, then the potential scanning was reversed at the same scanning rate until the test end.

The corrosion potential (E_{corr}) and corrosion current density (i_{corr}) were obtained using Tafel plots. The inhibition efficiency (IE%) was calculated using Equation:

$$\mathrm{IE}\ (\%) = \frac{\mathbf{i^0_{corr}} - \mathbf{i_{corr}}}{\mathbf{i^0_{corr}}} \times 100 \quad (4)$$

where i^0_{corr} and i_{corr} are the corrosion current density values in the test solutions without and with the inhibitors, respectively. In addition, the pitting potential (E_b) is the critical potential above which pitting corrosion starts on steel surface [36], the repassivation potential (E_{pp}) is the lowest potential for localized corrosion to propagate [38], and the pit transition potential (E_{ptp}) is a characteristic potential that is correlated with the repassivation at the pit bottom [39,44,45].

The EIS measurements were performed under the corrosion potential with a potential perturbation of 15 mV and the scanning frequency range was 100 kHz-0.01 Hz. The impedance data were fitted using ZSimpWin software. A three-electrode system was used in the electrochemical tests. A platinum electrode functioned as a counter electrode, the steel specimen worked as the working electrode, and the reference electrode was a saturated calomel reference electrode (SCE). Six parallel tests were run under each experimental condition.

An X-ray photoelectron spectroscopy (XPS) test was performed to analyze the surface composition with a Thermo Fisher ESCALAB 250 spectrometer (Qaltham, MA, USA). The samples were immersed in the carbonated SCP solution with different inhibitors for 24 h before XPS analysis. The binding energy values were calibrated using the C 1s peak at 248.8 eV.

To measure the wettability, the contact angle tests were performed on the inhibitor treated Q235 carbon steel surface using a JGW-36 contact angle test system (Chenghui Company, Chengde, China). During the test, the steel sample was mounted on the horizontal stage, the water drop (5 μL) was placed onto the steel surface using the syringe and the contact angle was measured using an integrated camera. For each sample, three distinct locations on the surface were measured and the average value was taken.

4. Conclusions

In carbonated SCP solution with 0.02 M NaCl, CLS could increase the pitting potential and decrease the corrosion current density for Q235 carbon steel, and the inhibition efficiency reaches 91.27% with 800 ppm CLS addition. Na_2MoO_4 also shows inhibition for both pitting and general corrosion, but the inhibition effect is obviously lower than that of CLS.

CLS and Na_2MoO_4 show a synergistic inhibition effect in the tested system. The compounded inhibitor can be defined as mix-type inhibitor. With 400 ppm CLS plus 600 ppm Na_2MoO_4, the pitting potential moves positively about 200 mV and the IE% reaches 92.67%. After 24 h immersion, the IE% further increases up to 99.2%.

XPS results confirm the adsorption of CLS and reveal the precipitation of oxides or hydroxides of Ca and Mo. Na_2MoO_4 could promote the stability of the passive film, and the insoluble molybdenum compounds and $CaO/Ca(OH)_2$, together with the adsorbed CLS, deposit on the steel surface, forming a complex film. The compounded film effectively inhibits corrosion of the steel surface.

Author Contributions: Investigation, B.L.; Supervision, Y.Z.; Writing—original draft, B.L.; Writing—review & editing, Y.Z.

Funding: This research was funded by the National Natural Science Foundation of China grant 51210001.

Acknowledgments: The authors would like to thank the National Natural Science Foundation of China (Contract 51210001) for support for this work.

Conflicts of Interest: The authors declare no conflict of interest.

References

1. Xu, H.; Liu, Y.; Chen, W.; Du, R.; Lin, C. Corrosion behavior of reinforcing steel in simulated concrete pore solutions: A scanning micro-reference electrode study. *Electrochim. Acta* **2009**, *54*, 4067–4072. [CrossRef]
2. Cao, Y.; Dong, S.; Zheng, D.; Wang, J.; Zhang, X.; Du, R.; Song, G.; Lin, C. Multifunctional inhibition based on layered double hydroxides to comprehensively control corrosion of carbon steel in concrete. *Corros. Sci.* **2017**, *126*, 166–179. [CrossRef]
3. Cao, F.; Wei, J.; Dong, J.; Ke, W. The corrosion inhibition effect of phytic acid on 20SiMn steel in simulated carbonated concrete pore solution. *Corros. Sci.* **2015**, *100*, 365–376. [CrossRef]
4. Anonymous. Draft recommendation for repair strategies for concrete structures damaged by reinforcement corrosion. *Mater. Struct.* **1994**, *27*, 415–436. [CrossRef]
5. Yang, Z.; Fischer, H.; Polder, R. Synthesis and characterization of modified hydrotalcites and their ion exchange characteristics in chloride-rich simulated concrete pore solution. *Cem. Concr. Compos.* **2014**, *47*, 87–93. [CrossRef]
6. Huet, B.; L'Hostis, V.; Miserque, F.; Idrissi, H. Electrochemical behavior of mild steel in concrete: Influence of pH and carbonate content of concrete pore solution. *Electrochim. Acta* **2005**, *51*, 172–180. [CrossRef]
7. Yang, Z.; Fischer, H.; Polder, R. Modified hydrotalcites as a new emerging class of smart additive of reinforced concrete for anticorrosion applications: A literature review. *Mater. Corros.* **2014**, *64*, 1066–1074. [CrossRef]
8. Jin, M.; Xu, J.; Jiang, L.; Xu, Y.; Chu, H. Investigation on the performance characteristics of chloride selective electrode in concrete. *Ionics* **2015**, *21*, 2981–2992. [CrossRef]
9. Hamdani, N.E.; Fdil, R.; Tourabi, M.; Jama, C.; Bentiss, F. Alkaloids extract of Retama monosperma (L.) Boiss. seeds used as novel eco-friendly inhibitor for carbon steel corrosion in 1 M HCl solution: Electrochemical and surface studies. *Appl. Surf. Sci.* **2015**, *357*, 1294–1305. [CrossRef]
10. Faustin, M.; Maciuk, A.; Salvin, P.; Roos, C.; Lebrini, M. Corrosion inhibition of C38 steel by alkaloids extract of Geissospermum laeve in 1M hydrochloric acid: Electrochemical and phytochemical studies. *Corros. Sci.* **2015**, *92*, 287–300. [CrossRef]
11. Heakal, E.T.; Elkholy, A.E. Gemini surfactants as corrosion inhibitors for carbon steel. *J. Mol. Liq.* **2017**, *230*, 395–407. [CrossRef]
12. Abdulrahman, A.S.; Ismail, M.; Hussain, M.S. Corrosion inhibitors for steel reinforcement in concrete: A review. *Sci. RES. Essays* **2011**, *6*, 4152–4162. [CrossRef]
13. Abdulrahman, A.S.; Ismail, M.; Hussain, M.S. Inhibiting sulphate attack on concrete by hydrophobic green plant extract. *Adv. Mater. Res.* **2011**, *250*, 3837–3843. [CrossRef]
14. Abdulrahman, A.S.; Ismail, M.; Hussain, M.S. Inhibition of corrosion of mild steel in hydrochloric acid by bambusa arundinacea. *Int. Rev. Mech. Eng.* **2011**, *5*, 59–63.
15. Tang, F.; Wang, X.; Xu, X.; Li, L. Phytic cid doped nanoparticles for green anticorrosion coatings. *Colloids Surf. A* **2010**, *369*, 101–105. [CrossRef]
16. Mohamed, H.A. Eco-friendly zero VOC anticorrosive paints for steel protection. *J. Appl. Polym. Sci.* **2012**, *125*, 1790–1795. [CrossRef]
17. Ouyang, X.; Qiu, X.; Lou, H.; Yang, D. Corrosion and Scale Inhibition Properties of Sodium Lignosulfonate and Its Potential Application in Recirculating Cooling Water System. *Ind. Engin. Chem. Res.* **2006**, *45*, 5716–5721. [CrossRef]
18. Macias, A.; Goñi, S. Characterization of admixture as plasticizer or superplasticizer by deflocculation test. *ACI Mater. J.* **1999**, *96*, 40–46.
19. Forostyan, Y.N.; Prosper, M. Inhibiting properties of lignin. *Chem. Nat. Compd.* **1983**, *19*, 358–359. [CrossRef]
20. Yahya, S.; Othman, N.K.; Daud, A.R.; Jalar, A. The inhibition of carbon steel corrosion by lignin in HCl and H_2SO_4, Universiti-kebangsaan-malaysia, Faculty-of-science-and-technology. *Am. Inst. Phys.* **2013**, *1571*, 132–135.
21. Akbarzadeh, E.; Ibrahim, M.N.M.; Rahim, A.A. Monomers of lignin as corrosion inhibitors for mild steel: Study of their behaviour by factorial experimental design. *Br. Corros. J.* **2012**, *47*, 302–311. [CrossRef]
22. Abu-Dalo, M.A.; Al-Rawashdeh, N.A.F.; Ababneh, A. Evaluating the performance of sulfonated Kraft lignin agent as corrosion inhibitor for iron-based materials in water distribution systems. *Desalination* **2013**, *313*, 105–114. [CrossRef]

23. Bishop, M.; Barron, A.R. Cement Hydration Inhibition with Sucrose, Tartaric Acid, and Lignosulfonate: Analytical and Spectroscopic Study. *Ind. Eng. Chem. Res.* **2006**, *45*, 7042–7049. [CrossRef]
24. Li, R.; Yang, D.; Guo, W.; Qiu, X. The adsorption mechanisms of sodium lignosulfonate on Al_2O_3 particles in aqueous solution. *Adv. Chem. Eng.* **2012**, *550–553*, 1120–1123. [CrossRef]
25. Wang, Y.; Zuo, Y.; Zhao, X.; Zha, S. The adsorption and inhibition effect of calcium lignosulfonate on Q235 carbon steel in simulated concrete pore solution. *Appl. Surf. Sci.* **2016**, *379*, 98–110. [CrossRef]
26. Emregül, K.C.; Aksüt, A.A. The effect of sodium molybdate on the pitting corrosion of aluminum. *Corros. Sci.* **2003**, *45*, 2415–2433. [CrossRef]
27. Bai, W.; Li, X.; Mu, G.; Qu, Q. Molybdate and tungstate as corrosion inhibitors for cold rolling steel in hydrochloric acid solution. *Clean. World* **2006**, *48*, 445–459.
28. Kumari, V.A.; Sreevalsan, K.; Shibli, S.M.A. Sodium molybdate for the effective protection of steel: A comprehensive review. *Corros. Prev. Contro.* **2001**, *48*, 83–109.
29. Zhou, Y.; Zuo, Y. The inhibitive mechanisms of nitrite and molybdate anions on initiation and propagation of pitting corrosion for mild steel in chloride solution. *Appl. Surf. Sci.* **2015**, *353*, 924–932. [CrossRef]
30. Cheng, T.; Lee, J.; Tsai, W. Passivation of titanium in molybdate-containing sulphuric acid solution. *Electrochim. Acta* **1991**, *36*, 2069–2076. [CrossRef]
31. Atia, A.A.; Donia, A.M.; Awed, H.A. Synthesis of magnetic chelating resins functionalized with tetraethylenepentamine for adsorption of molybdate anions from aqueous solutions. *J. Hazard. Mater.* **2008**, *155*, 100–108. [CrossRef] [PubMed]
32. Loto, R.T. Study of the synergistic effect of 2-methoxy-4-formylphenol and sodium molybdenum oxide on the corrosion inhibition of 3CR12 ferritic steel in dilute sulphuric acid. *Result. Phys.* **2017**, *7*, 769–776. [CrossRef]
33. Zhou, Y.; Zuo, Y.; Lin, B. The compounded inhibition of sodium molybdate and benzotriazole on pitting corrosion of Q235 steel in NaCl+$NaHCO_3$, solution. *Mat. Chem. Phys.* **2017**, *192*, 86–93. [CrossRef]
34. Ferreira, E.S.; Giacomelli, C.; Giacomelli, F.C.; Spinelli, A. Evaluation of the inhibitor effect of l-ascorbic acid on the corrosion of mild steel. *Mat. Chem. Phys.* **2004**, *83*, 129–134. [CrossRef]
35. Bouanis, M.; Tourabi, M.; Nyassi, A.; Zarrouk, A.; Jama, C.; Bentiss, F. Corrosion inhibition performance of 2,5-bis(4-dimethylaminophenyl)-1,3,4-oxadiazole for carbon steel in HCl solution: Gravimetric, electrochemical and XPS studies. *Appl. Surf. Sci.* **2016**, *389*, 952–966. [CrossRef]
36. Standard test method for conducting cyclic potentiodynamic polarization measurements for localized corrosion susceptibility of iron-, nickel-, or cobalt-based alloys, ASTM-G61-86. In *Annual Book of ASTM Standards*; ASTM Internationa: Philadelphia, PA, USA, 1999; pp. 239–242.
37. Tiziano, B.; Giampaolo, G.; Gabriella, R. Study of stainless steels corrosion in a strong acid mixture. Part 1: Cyclic potentiodynamic polarization curves examined by means of an analytical method. *Corros. Sci.* **2018**, *130*, 113–125.
38. Blin, F.; Koutsoukos, P.; Klepetsianis, P.; Forsyth, M. The corrosion inhibition mechanism of new rare earth cinnamate compounds—Electrochemical studies. *Electrochim. Acta* **2007**, *52*, 6212–6220. [CrossRef]
39. Ou, H.H.; Tran, Q.T.P.; Lin, P.H. A synergistic effect between gluconate and molybdate on corrosion inhibition of recirculating cooling water systems. *Corros. Sci.* **2018**, *133*, 231–239. [CrossRef]
40. Refaey, S.A.M.; El-Rehim, S.S.A.; Taha, F.; Saleh, M.B.; Ahmed, R.A. Inhibition of chloride localized corrosion of mild steel by PO_4^{3-}, CrO_4^{2-}, MoO_4^{2-}, and NO_2^- anions. *Appl. Surf. Sci.* **2000**, *158*, 190–196. [CrossRef]
41. Eghbali, F.; Moayed, M.H.; Davoodi, A.; Ebrahimi, N. Critical pitting temperature (CPT) assessment of 2205 duplex stainless steel in 0.1 M NaCl at various molybdate concentrations. *Corros. Sci.* **2011**, *53*, 513–522. [CrossRef]
42. Ilevbare, G.O.; Burstein, G.T. The inhibition of pitting corrosion of stainless steels by chromate and molybdate ions. *Corros. Sci.* **2003**, *45*, 1545–1569. [CrossRef]
43. Moayed, M.H.; Newman, R.V. Aggressive effects of pitting 'inhibitors' on highly alloyed stainless steels. *Corros. Sci.* **2006**, *48*, 3513–3530. [CrossRef]
44. Trasatti, S.P. Electrochemical approach to repassivation kinetics of Al alloys: Gaining insight into environmentally assisted cracking: Corrosion Reviews. *Corros. Rev.* **2015**, *33*, 373–393.
45. Trueba, M. The repassivation response from single cycle anodic polarization: The case study of a sensitized Al-Mg alloy. *Electrochim. Acta* **2018**, *259*, 492–499. [CrossRef]

46. Vukasovich, M.S.; Farr, J.P.G. Molybdate in corrosion inhibition—A review. *Polyhedron* **1986**, *5*, 551–559. [CrossRef]
47. Tang, Y.; Zuo, Y.; Wang, J.; Zhao, X.; Niu, B.; Lin, B. The metastable pitting potential and its relation to the pitting potential for four materials in chloride solutions. *Corros. Sci.* **2014**, *80*, 111–119. [CrossRef]
48. Danaee, I.; Khomami, M.N.; Attar, A.A. Corrosion behavior of AISI 4130 steel alloy in ethylene glycol–water mixture in presence of molybdate. *Mat. Chem. Phys.* **2012**, *135*, 658–667. [CrossRef]
49. Samiento-Bustos, E.; Rodriguez, J.G.G.; Uruchurtu, J.; Dominguez-Patiño, G.; Salinas-Bravob, V.M. Effect of inorganic inhibitors on the corrosion behavior of 1018 carbon steel in the LiBr + ethylene glycol + H_2O mixture. *Corros. Sci.* **2008**, *50*, 2296–2303. [CrossRef]
50. Zhang, F.; Pan, J.; Claesson, P.M. Electrochemical and AFM studies of mussel adhesive protein (Mefp-1) as corrosion inhibitor for carbon steel. *Electrochim. Acta* **2011**, *56*, 1636–1645. [CrossRef]
51. Zhang, Z.; Tian, N.; Zhang, W.; Huang, X.; Ruan, L.; Wu, L. Inhibition of carbon steel corrosion in phase-change-materials solution by methionine and proline. *Corros. Sci.* **2016**, *111*, 675–689. [CrossRef]
52. Breslin, C.B.; Treacy, G.; Carroll, W.M. Studies on the passivation of aluminium in chromate and molybdate solutions. *Corros. Sci.* **1994**, *36*, 1143–1154. [CrossRef]
53. Lopez-Garrity, O.; Frankel, G.S. Corrosion Inhibition of Aluminum Alloy 2024-T3 by Sodium Molybdate. *Corrosion -Houston Tx-* **2014**, *70*, 928–941. [CrossRef]
54. Han, P.; Li, W.; Tian, H.; Gao, X.; Ding, R.; Xiong, C.; Chen, C. Designing and fabricating of time-depend self-strengthening inhibitor film: Synergistic inhibition of sodium dodecyl sulfate and 4-mercaptopyridine for mild steel. *J. Mol. Liq.* **2018**, *268*, 425–437. [CrossRef]
55. Zhou, B.; Wang, Y.; Zuo, Y. Evolution of the corrosion process of AA 2024-T3 in an alkaline NaCl solution with sodium dodecylbenzenesulfonate and lanthanum chloride inhibitors. *Appl. Surf. Sci.* **2015**, *357*, 735–744. [CrossRef]
56. Tourabi, M.; Nohair, K.; Nyassi, A. Thermodynamic characterization of metal dissolution and inhibitor adsorption processes in mild steel/3,5-bis(3,4-dimethoxyphenyl)-4-amino-1,2,4-triazole/hydrochloric acid system. *J. Mater. Enviro. Sci.* **2014**, *5*, 1133–1143.
57. Gerónimo-López, C.; Vazquez-Arenas, J.; Picquart, M.; Picquart, M.; Gonzáleza, I. The energetic conditions determining the active dissolution of carbon steel during electrocoagulation in sulfate media. *Electrochim. Acta* **2014**, *136*, 146–156. [CrossRef]
58. Hirschorn, B.; Orazem, M.E.; Tribollet, B.; Vivier, V.; Frateur, I.; Musiani, M. Determination of effective capacitance and film thickness from constant-phase-element parameters. *Electrochim. Acta* **2010**, *55*, 6218–6227. [CrossRef]
59. Xun-jie, G.; Yu-chun, L.; Ke-ru, P. Electrochemical behavior of molybdate inhibitor in tap water. *Corros. Sci. Prot. Technol.* **2001**, *13*, 208–210.
60. Frateur, I.; Carnot, A.; Zanna, S.; Marcus, P. Role of pH and calcium ions in the adsorption of an alkyl N-aminodimethylphosphonate on steel: An XPS study. *Appl. Surf. Sci.* **2006**, *252*, 2757–2769. [CrossRef]
61. Olivares, O.; Likhanova, N.V.; Gómez, B.; Navarrete, J.; Llanos-Serrano, M.E.; Arce, E.; Hallen, J.M. Electrochemical and XPS studies of decylamides of α-amino acids adsorption on carbon steel in acidic environment. *Appl. Surf. Sci.* **2006**, *252*, 2894–2909. [CrossRef]
62. Pang, X.; Ran, X.; Fei, K.; Xie, J.; Hou, B. Inhibiting Effect of Ciprofloxacin, Norfloxacin and Ofloxacin on Corrosion of Mild Steel in Hydrochloric Acid. *Chin. J. Chem. Eng.* **2010**, *18*, 337–345. [CrossRef]
63. Dong, Z.H.; Shi, W.; Guo, X.P. Localized Corrosion Inhibition of Carbon Steel in Carbonated Concrete Pore Solutions Using Wire Beam Electrodes. *Acta Phys. Chim. Sin.* **2011**, *27*, 127–134.
64. Nakayama, N. Inhibitory effects of nitrilotris (methylenephosphonic acid) on cathodic reactions of steels in saturated $Ca(OH)_2$ solutions. *Corros. Sci.* **2000**, *42*, 1897–1920. [CrossRef]
65. Clayton, C.R.; Lu, Y.C. A bipolar model of the passivity of stainless steels - III. The mechanism of MoO_4^{2-} formation and incorporation. *Corros. Sci.* **1989**, *29*, 881–898. [CrossRef]
66. Muñoz, A.I.; Antón, J.G.; Nuévalos, S.L.; Guiñón, J.L.; Herranz, V.P. Corrosion studies of austenitic and duplex stainless steels in aqueous lithium bromide solution at different temperatures. *Corros. Sci.* **2004**, *46*, 2955–2974.
67. Temesghen, W.; Sherwood, P.M. Analytical utility of valence band X-ray photoelectron spectroscopy of iron and its oxides, with spectral interpretation by cluster and band structure calculations. *Anal. Bioanal. Chem.* **2002**, *373*, 601–608. [CrossRef] [PubMed]

68. Sajid, H.U.; Kiran, R. Influence of corrosion and surface roughness on wettability of ASTM A 36 steels. *J. Constr. Steel Res.* **2018**, *144*, 310–326. [CrossRef]
69. Datta, A.; Mukherjee, S. *Structural and Morphological Evolution in Metal-Organic Films and Multilayers*; CRC Press: Boca Raton, FL, USA, 2015.
70. Liang, C.; Lv, Z.; Zhu, Y.; Xu, S. Molybdate-based conversion treatment for improving the peeling strength between aluminum foil and polypropylene grafted with glycidyl methacrylate. *Surf. Coat. Technol.* **2014**, *249*, 1–5. [CrossRef]
71. Rutland, M.W.; Parker, J.L. Surfaces Forces between Silica Surfaces in Cationic Surfactant Solutions: Adsorption and Bilayer Formation at Normal and High pH. *Langmuir* **1994**, *10*, 1110–1121. [CrossRef]
72. Yu, H.; Chiang, K.T.K. Threshold chloride level and characteristics of reinforcement corrosion initiation in simulated concrete pore solutions. *Construct. Build. Mat.* **2012**, *26*, 723–729. [CrossRef]

Sample Availability: Samples of the compounds are available from the authors.